Structural and transport properties of $ZrTe_2$ single crystals

D. N. BHAVSAR[*], A. R. JANI[#]
[*]*Shree Sahajanad School of Science and Commerce, Visnagar-384315, Gujarat, India*
[#]*Department of Physics, Sardar Patel University, Vallabh Vidyanagar-388120, Gujarat, India*

We report measurements of the structural and transport properties of $ZrTe_2$ single crystal and find this to be characteristic of a semimetal with hexagonal crystalline phase. We consider that this semi metallic behavior arises from a small overlap of the tellurium *p* valence band and the zirconium *d* conduction band. Thermoelectric power shows the diffusion of holes are greater compared to electrons from hot to cold end. Measurement of the resistivity shows an increase in the band overlap and carrier concentration with pressure. Surface microstructure analysis done on various samples of $ZrTe_2$ shows the presence of step growth.

(Received November 26, 2012; accepted January 22, 2014)

Keywords: Single Crystal, CVT method, PXRD, High Pressure, Resistivity

1. Introduction

The disulphide, ditellurides and diselenides of Sn, Ti, Zr, and Hf are members of group of compounds which crystallize in the space group $P\bar{3}m1$ with the characteristic CdI_2 type structure. Layered 4d transition metal dichalcogenides of group IV, V and VIB metals exhibit semiconducting or metallic properties. Among them, materials of the same group generally show similar electrical, magnetic and optical behaviors [1]. Many theoretical calculations support the validity of the rigid band model for the compound with the same metal co-ordination. Thermoelectric materials have acquired increased attention by researchers owing to the unique capability of such materials to convert heat directly in to the electricity. Etch pit studies of these single crystal materials suggested that their dislocation densities might be unusually low, and study of dislocation distribution in the single crystals of the compounds has been made by X-Ray topography using both Lang technique and X-Ray topography. Most of the group IV dichalcogenides are semiconductors, with a band gap between the top of the filled chalcogen p band and the bottom of the transition-metal d band. This is the case for HfS_2, $HfSe_2$, ZrS_2, $ZrSe_2$ and TiS_2 [2, 3]. However, there is evidence for a small overlap, of about 100 meV, between the p and d bands in $TiSe_2$ both from the pressure dependence of the conductivity and Hall coefficient [2] and from angle-resolved photo-emission [4]. $TiTe_2$ shows a larger band overlap of ~0.6 eV [5], and an overlap of ~0.2eV has been predicted for $HfTe_2$ by [6] by extrapolation of the trend of the band gap with the in-plane lattice parameter from $HfS_2$and $HfSe_2$.

2. Experimental

Polycrystalline material of $ZrTe_2$ has been synthesized from elements in powder or granular forms (Zr and Te: Alfa Aesar Company, USA) using quartz ampoule sealed under the vacuum level 10^{-5} torr. The quartz ampoule was carefully degreased with Ajax, etched (HF 40%) and dried for two days (using oven) before introducing any reactants in it. After this sealing, the sealed ampoule was placed in dual zone horizontal furnace. During synthesis, the temperature was increased very slowly up to 800 ^{0}C in approximately 27 hrs to avoid any explosion of the ampoule. Then, the system has been kept at constant temperature (800 ^{0}C) for 30 hrs, and then slowly cooled down to room temperature in 22 hrs. The product (polycrystalline form of $ZrTe_2$ material) was recovered after opening the ampoule. After fine milling of the product (using Agate Mortar), samples were reintroduced in a new quartz ampoule and sealed under secondary vacuum of 10^{-5} torr and then placed in the dual zone horizontal furnace with growth zone at 800 ^{0}C and source at 850 ^{0}C for 90 hrs with uniform temperature gradient of 50 ^{0}C throughout the process. After this, the furnace was slowly cooled down at room temperature in 17 hrs. The as grown crystals are hexagonal platelets with a metallic luster and characteristic dimensions of 5 × 5 × 0.1 mm^3. The stoichiometric composition of the as-grown CVT single crystal was studied through energy dispersive analysis of X-rays (EDAX) attached to Philips ESEM. Chemical analysis showed the presence of 1 at. % excess Te. The crystallographic parameters were determined through the X-ray diffraction (XRD) obtained by means of a Philips X-ray diffractometer (X-pert-MPD) employing

CuK_α radiations. Thermoelectric power set-up established in laboratory is used to measure the thermoelectric power of the $ZrTe_2$ single crystal. This experimental set-up consists of two assemblies: one is the sample chamber with two heaters and pickup probes and the other is electronic circuits to control the temperature and also the temperature gradient across the sample. The temperature is measured by the thermocouple and the gradient is measured by the differential temperature sensor. The sample is directly mounted on the two heaters and by applying the temperature gradient between two ends of the sample, the thermoelectric power is generated which is measured by Digital Voltmeter of Keithly. Electrical resistivity was measured in the temperature range of 308K-533Kwith a four-probe apparatus of the type commonly used in semiconductor work. Several readings were taken over different regions of specimen and consistent results were obtained in each instance. For surface microstructure analysis of $ZrTe_2$ single crystal, optical microscope of Carl Zeiss made is used. Different shapes and size of the samples are used for the microstructure analysis. The room temperature (300K) dc resistivity measurements as a function of pressure were taken up to 8 GPa. Pressure was generated with a Bridgman-type tungsten carbide opposed anvil (face diameter of 11.3 mm) apparatus with an insitu Bismuth (purity 99.999%) pressure calibration. The pressure corresponding to the load at the minimum in the resistivity curve in Bi II phase was assigned the value 2.52GPa, which is the average of Bi I–II and Bi II–III transition pressures. Similarly, the pressure corresponding to the load at the mid-point of Bi III–IV transition was taken to be 7.75 GPa [7]. A smooth curve through the origin and these fixed pressure points provided calibration to 8GPa.

3. Results and discussion

Fig. 1. shows the powder XRD pattern for $ZrTe_2$ compound. Like many of the early transition-metal dichalcogenides, $ZrTe_2$ adopts the 1H-CdI_2 structure, which has a hexagonal close packing of anions with the metal atoms in octahedral holes. The space group for this structure is $P\bar{3}m1$ (D^3_{3d}). The comparison of XRD pattern with standard reveals that the material possesses the hexagonal phase. Sharp and less numbers of peaks suggested the good crystallinity and fewer impurities of the sample. The relative intense peak observed at $2\theta=27.68^0$, corresponding to the hexagonal (002) plane. All other peaks which are shown in the pattern are also corresponding to hexagonal phase which are in good agreement with the reported value [8]. The lattice parameters of hexagonal phase were determined by standard relation. The lattice parameters are given in the Table 1.

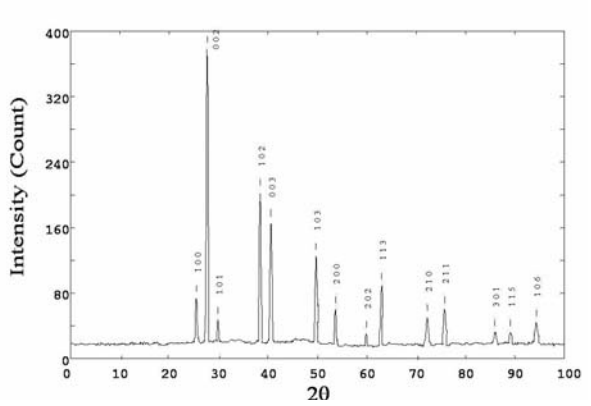

Fig. 1. The powder X-Ray Diffraction pattern for $ZrTe_2$ compound.

Table 1. Lattice parameters for compound of $ZrTe_2$ obtained from powder XRD pattern.

Compound	a (Å)	b (Å)	c (Å)	Volume ($Å^3$)	c/a
$ZrTe_2$	3.95	3.95	6.54	88.369	1.65

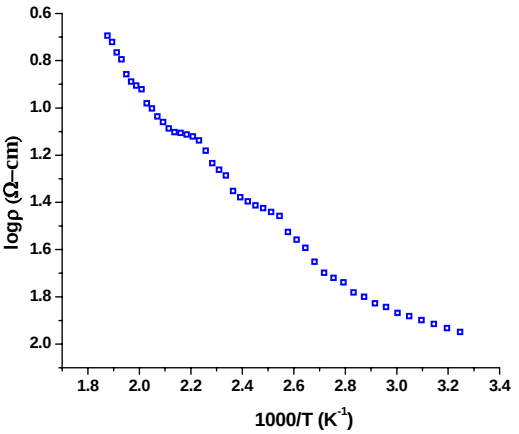

Fig. 2. Logarithm variation of dc electrical resistivity with inverse of the temperature for $ZrTe_2$ single crystal.

Materails possesing narrow band gaps in the vicinity of the Fermi energy are prone to electron-phonon coupling. Such interactions originates lattice distortions that move with electrons in the crystal lattice originating the mobility drop at the low temperature [9]. The two-slope resistivity logarithm vs. inverse temperature plot shown in Fig. 2. is characteristic of electron-phonon coupling in which transport at low temperatuere occurs by means of thermally activated jumps of polarons [10-12] from site to site. Mott [13] indicated that materials which are intrinsic semiconductors like the chalcogenide glasses, the valance and conduction bands will exist with a range of weakly localized states at the bottom, along with a tail

of strongly localized states due to structural defects, which originate the impurity conduction mechanism at low temperature. Therefore, the resistivity behaving like

$$\ln\rho = A + \frac{B}{T^{1/4}} \quad (1)$$

Such conduction mechanism found in semiconductors whose electrical conductivity at low temperature is mainly determined by impurities, given the strong localization of the density of states at the impurity levels as it has been pointed out by Mott [13].

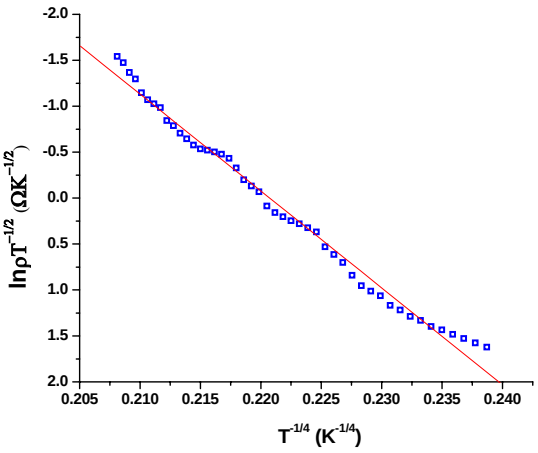

Fig. 3. Variable-range-hopping fits to dc electrical resistivity data of the$ZrTe_2$ single crystal.

At higher temperature, the Fermi level shifts away from the impurity region, where conduction by hopping is the main mechanism, and the energy available allows for transitions from the localized impurity states to the conduction band that will give rise to lower resistivity values and a deviation from the linear dependence with $T^{-1/4}$ (see Fig. 3.). It is worth emphasizing the fact that the model also assumes strongly disordered systems, which is a plausible assumption in the narrow gap impurity semiconductors under investigation, where crystallographic faults and/or small amounts of impurities dissolved in the bulk phase may account for the randomness and localization necessary for the VRH mechanism to take place.

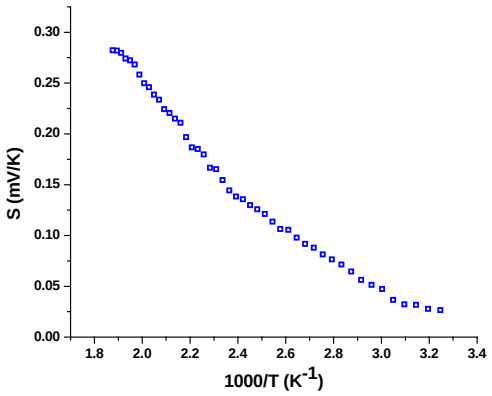

Fig. 4. Variation of thermoelectric power with inverse of temperature.

The increasing Seebeck coefficient as the temperature rises confirms the existence of an undetermined number of impurity levels (p-type) close to the valance band. A slope change is observed at higher temperature about 473K (see Fig. 4.) not seen in the resistivity vs. temperature plot regarding the fact that the Seebeck coefficient is a means of probing the density of states near the Fermi energy. The behavior of the Seebeck coefficient of $ZrTe_2$ is explained by the existence of a metallic impurity band, i.e. possessing the high degree of overlapping near the Fermi energy that has the overall effect of reducing absolute value of the Seebeck coefficient and conversely narrow impurity bands possessing low electron mobility and large effective masses will enhance the total Seebeck coefficient. Therefore the same formula used to explain the Seebeck coefficient of metals can be used to explain the Seebeck coefficient of degenerate semiconductors with metallic impurity bands.

$$S = \frac{\Pi^2}{3}\frac{k_B{}^2 T}{e}\left\{\frac{d(\ln\sigma)}{dE}\right\}_{E=E_F} \quad (2)$$

In the above equation, the density of states is the predominating terms. The anomaly observed in the thermo power of $ZrTe_2$ can be explained in terms of a wide metallic impurity band that confirms the low electrical resistivity and low and metal like Seebeck coefficient value. A wider impurity band will originate more carriers delocalization and a smaller derivative values in above equation, accounting for the low Seebeck observed for this compound. Thus, as the temperature rises the Fermi energy will dwell longer close to the metal like band, thereby expanding the temperature range at which the conduction may occur supporting the existence of this wide metallic impurity band in $ZrTe_2$ is the fact that the linear fit to the Seebeck data intercepts the y-axis at the origin.

The variation of lnρ with pressure up to 7 GPa is shown in Fig. 5. The resistivity falls smoothly with pressures up to 0.4 GPa and again it starts decreasing for

higher pressure until the steady pressure has been reached. The decrease in resistivity with pressure indicates that there is an increase in band overlap with pressure means as the pressure increases the material become more and more metallic. We assume that the variation of the resistivity with pressure is due primarily to an increase in carrier concentration. The decrease in the resistivity is very low [14,15].

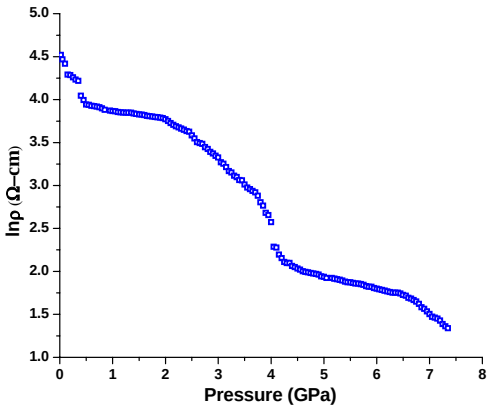

Fig. 5. Variation of lnρ with Pressure.

In the case of high concentration of impurity, impurity band is likely to be formed in place of stabilized impurity level. The density of electronic states follows the density of states of phonons when there is strong electron–phonon coupling. The phonon density of states is given by

$$D(\omega) = A\omega^2 \tag{3}$$

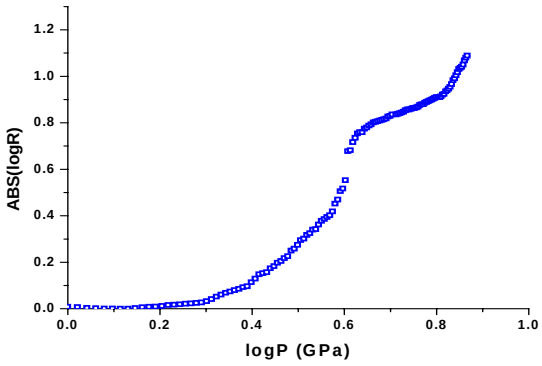

Fig. 6. Variation of logρ with logP.

within the Debye approximation. The electrical resistivity is proportional to the carrier concentration, which is in turn proportional to the density of states. The total number of filled states is given by,

$$n(\omega) = \int D(\omega)d\omega = \frac{A\omega^3}{3} + B \tag{4}$$

Now, the phonon frequency is varying with applied pressure as $\omega \sim \sqrt{P}$ for acoustic phonons and $\omega \sim P$ for optical phonons [14-16]. This leads to $\rho \sim \omega^3 \sim P^{3/2}, \rho \sim \omega^5 \sim P^{5/2}$. If the slope, $s = 0.5$, it indicates band conduction, if $s = 1.0$ it indicates hopping conduction and if $s = 3.0$ (see Fig. 6.) then it indicates inter-band conduction. Thus, in our case the slope varies from 0.201 to 1.15 for $ZrTe_2$ samples, which clearly indicates band conduction and hopping conduction to be dominant in these samples.

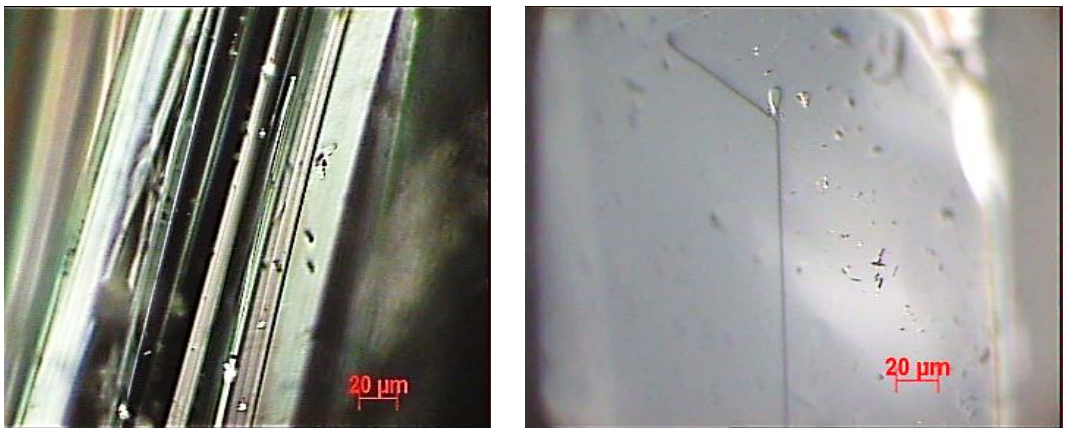

a b

Fig. 7(a) (Color Online). Step growth on surface of $ZrTe_2$ single crystal. (b). Directional dependent growth on the faces of $ZrTe_2$ single crystal.

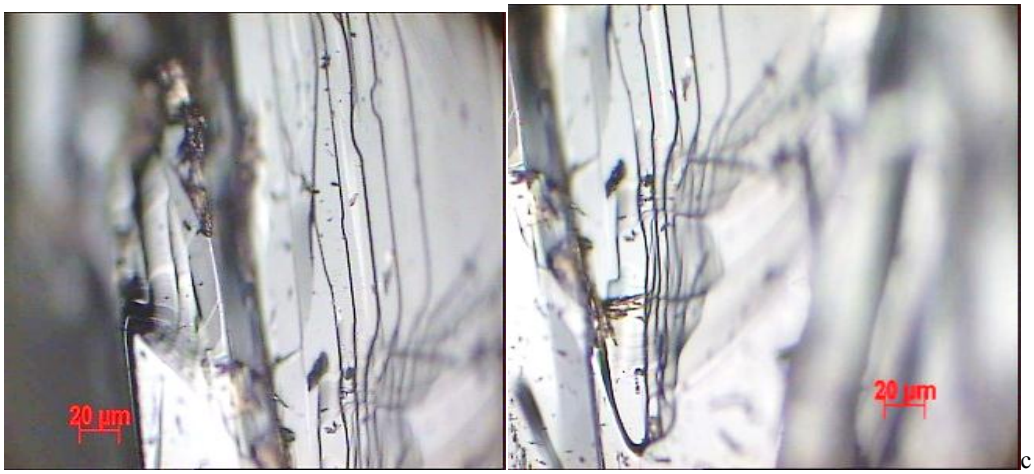

c

Fig. 7(c) (Color Online). Irregular shaped crystal blocks on the surface of $ZrTe_2$ single crystals.

Fig. 7 (a,b,c). shows the surface microstructures of $ZrTe_2$ single crystals. Fig. 7a shows the step growth of $ZrTe_2$ single crystals. Theory of crystal growth mechanism predicts that stepped crystal results from the three processes:

1. Transport of molecules from the vapor to the surface; 2. diffusion of adsorbed molecules to the steps; and 3. diffusion of molecules along the edge of a step to a kink.

Now the rate of advance of straight step is,

$$V = 2(\sigma - 1) X_s v e^{\frac{-w}{k_B T}} \quad (5)$$

where $(\sigma-1)$ is the super saturation, X_s is the mean distance that a molecule wonder over the time over the surface of the crystal between the time it strikes and the time it evaporates, v is an atomic vibration frequency factor and *w* is the evaporation energy. If $X_s >> X_0$ means mean distance between kinks X_0 is very small compared to X_s then the molecules have high probability of adhering to the step if adsorbed near it, regardless of the orientation of the step.

When the rate of advancement of step is dependent on crystal face orientation, a directional dependence of macroscopic growth will be observed. When $X_s >> X_0$ is no longer true then the directional growth results, the edge of the steps becoming straight and perpendicular to the slow growth direction. Example of this is shown in the fig. 7(a,b).

Fig. 7(c) shows the region near an edge of a crystal block, cleaved out. A block pattern is apparent. The blocks are neither flat, nor are their surfaces parallel. This is a fairly characteristic picture and many like it have been obtained from different samples [17].

3. Conclusions

Single crystals of $ZrTe_2$ have been successfully grown by chemical vapour transport technique. The powder XRD pattern confirms the hexagonal phase of the grown material. Measurements of high temperature and pressure dependent resistivity confirm the semimetal nature of the grown crystals. The metallic impurity conduction mechanism is observed from the high temperature resistivity and thermoelectric power measurements. $ZrTe_2$ is a semimetal and that at ambient pressure it does not show any of the structural instabilities which is commonly observed in materials with similar layer structures. High pressure resistivity also tells the band conduction and hopping conduction mechanism is present in the crystal. Directional dependent growth is observed for $ZrTe_2$ crystals. Due to this step growth is dominant in this material.

Acknowledgement

D. N. Bhavsar is very much thankful to DST for selection on INSPIRE Fellowship and providing necessary financial support to carry out this work as a full time Ph.D. student.

References

[1] J. A. Wilson, A. D. Yoffe, Adv. Phys. **18**, 193 (1969).
[2] A. R. Beal, J. C. Knights, W. Y. Liang, J. Phys. C: Solid State Phys. **5,** 3531 (1972).
[3] P. C. Klipstein, A. G. Bagnall, W. Y. Liang, E. A. Marseglia, R. H. Friend, J. Phys. C: Solid State Phys. **14,** 4067 (1981).
[4] C. M. Fang, R. A. de Groot, C. Haas, Phys. Rev. B. **56**(8), 4455 (1997).
[5] D. K. G. de Boer, C. F. van Bruggen, G. W. Bus, R. Coehoorn, C. Haas, G. A. Sawatsky, H. W. Myron, D. Norman H. Padmore, Phys. Rev. B **29**, 6797 (1984).
[6] S. Bayliss, W. Y. Liang, 1982 J. Phys. C: Solid State Phys. **15,** 1283 (1972).
[7] M. Dave, R. Vaidya, S. G. Patel, A. R. Jani, Bull. Mater. Sci.**27**, 213 (2004).

[8] W. G. R. Wyckoff, Crystal Structures, **vol. 1**, second ed., pp. 269 (1965).
[9] J. G. C. Kennedy, P. N. LaMori, J. Geophys. Res. **67**, 851 (1962).
[10] A. H. Reshak, S. Auluck, Phys. Rev. B **68,** 245113 (2003).
[11] D. Adler, J. Feinleib, Phys. Rev. B, **2**(8), 3112 (1970).
[12] H. Böttger, V. Bryksin, Hopping conduction in solids, (Akademie- Verlag, Berlin, 1985).
[13] N. F. Mott, Conduction in non-crystalline materials, Philos. Mag., **19**(160), 835 (1969).
[14] A. T. Oza, Indian. J. Phys. **73A**, 373 (1999).
[15] A. T. Oza, P. C. Vinodkumar, Indian. J. Phys. **72A**, 171 (1998).
[16] D. N. Bhavsar, M.Phil. Dissertation, Sardar Patel University, Vallabh Vidyanagar, (2010).
[17] J. J. Gilman, The Art and Science of Growing Crystals (John Wiley & Sons, Inc; New York) (1963).

*Corresponding author: div.bhavsar@gmail.com